RSC Advances

ROYAL SOCIETY OF CHEMISTRY

www.rsc.org/advances

A Facile One-step Method to Synthesize SiO_2@Polydopamine Core-shell Nanospheres for Shear Thickening Fluid

Mei Liu[a], Wanquan Jiang[a,], Qian Chen[b], Sheng Wang[a], Ya Mao[a], Xinglong Gong[b,]*, Ken Cham-Fai Leung[c], Jie Tian[d], Huijuan Wang[d], Shouhu Xuan[b,]**

[a]*Department of Chemistry, Collaborative Innovation Center of Suzhou Nano Science and Technology, University of Science and Technology of China (USTC), Hefei 230026, PR China*
[b]*CAS Key Laboratory of Mechanical Behavior and Design of Materials, Department of Modern Mechanics, USTC, Hefei 230027, PR China*
[c]*Department of Chemistry and Institute of Creativity, Hong Kong Baptist University, Kowloon, Hong Kong SAR, P. R. China.*
[d]*Engineering and Materials · Science · Experiment Center, USTC, Hefei 230027, PR China*

[*]Corresponding author: Tel: 86-551-63607605; Fax: 86-551-63600419.

E-mail: jiangwq@ustc.edu.cn (W.Q. Jiang)

gongxl@ustc.edu.cn (X.L. Gong)

xuansh@ustc.edu.cn (S.H. Xuan)

ABSTRACT: A facile one-step method was developed to synthesize core shell structured SiO_2@Polydopamine (PDA) nanospheres. During the synthesis, the PDA shell was simultaneously coated on the SiO_2 nanospheres to form the core shell nanostructure. The PDA shell thickness was tunable by varying the concentration of the starting dopamine precursor. After dispersing the core shell nanospheres into the polyethylene glycol 200, the SiO_2@PDA based shear thickening fluid (STF) was obtained. In comparison to the pristine SiO_2, the SiO_2@PDA based STF presented better ST effects and its maximum viscosity can reach to as high as 194.6 Pa·s. A possible enhancing mechanism was proposed to investigate the structural dependent ST effect. This high performance SiO_2@PDA based STF would be widely applied in body armor and safe-guarding area.

1. INTRODUCTION

Shear-thickening (ST) is a type of Non-Newtonian flow behavior in concentrated suspensions, of which the viscosity increases dramatically when encountering an unexpected force. If the applying shear or striking beyond the critical value, the fluids become thickening and even transformed from liquid state to solid-like state[1-4]. Due to this unique reversible ST effect, the ST fluids (STFs) attracted widely applications in damper, "liquid" armor, impact absorbers, control devices, sports shoe cushioning, and rotary speed limiters, etc[4-7]. It was claimed that the shear thickening was originated from the hydrodynamic lubrication forces between the dispersing particles[8-11]. Various techniques such as the Rheo-optical and neutron scattering, Flow-ultra small angle neutron scattering, and fast confocal rheology measurements supported the above mechanism[9, 10, 12, 13].

During the past decades, much effort has been conducted to prepare high performance STFs and investigate their structure dependent rheological properties. The previous work indicated that the mechanical characteristics of the STFs were influenced by dispersing particles, carrying fluids, and the additives[14-20]. Among them, the dispersing particles played as the critical role. A large amount of natural materials such as the calcium carbonate, silica, alumina, titania, barium sulfate,[21] blood cells, cornstarch particles[4], starch particles[22] were effective for the STFs. Recently, to achieve the high performance STFs, the man-made particles such as polyvinylchloride (PVC), poly(styrene–acrylonitrile) (PS–AN), polystyrene (PSt)][4], polymethylmethacrylate (PMMA)[12], poly(styrene–ethyl acrylate) (PS–EA)[23], and

carbon nanofibers[24] were introduced into the ST area. Due to their tunable hardness, charges and elastic surface, these particles became attractive in STFs since they usually exhibited strong ST behavior[23].

The characteristic of the particles play an important role in determining the ST effect[25]. As soon as the yield strain is reached, the hard particles collide to each other and lead to the shear thickening. However, the shear thickening was damped by the thick outer shell in soft particles[26]. Recently, our group investigated the influence of particles' structure on the behavior of STF by synthesizing different structure PS-AA (polystyrene-acrylic acid) nanospheres. We found that particles with proper hard core and soft shell exhibited excellent shear thickening behavior[27]. The soft shell would contribute to increase the lubrication hydrodynamic interaction among the dispersing particles, therefore particle clusters would be formed much easier. The hard core of the nanospheres ensured the formed clusters could resist larger imposed stress. Therefore, it was proposed that the ideal dispersing particle for high performance STF should possess a hard core and a soft shell[4, 27].

Core shell particles are of specific research interests because they can integrate two or three different functionalities together into one material[28, 29]. During the past decade, various core shell particles such as the inorganic core/inorganic shell, inorganic core/polymer shell, and polymer core/polymer shell were reported for the application of biology, energy, separation, catalysis and etc. The *in situ* coating[30, 31], layer by layer[32-34], and one-pot method were the mostly favorable method for preparing the core/shell nanospheres[35-37]. Due to the in-compatibility between the

inorganic material and polymer, complicated procedures [38, 39] were often required in fabricating the core shell particles with inorganic core/polymer shell. Moreover, the scale of traditional method for the core/shell nanospheres was usually small[39, 40]. There are some typical works about preparation of core-shell particles, in which the scale of the products was small and the maximum scale does not exceed 5g[41-45]. However, the scale of required particles in the STF was relatively large. Therefore, a facile one-step method for preparing the inorganic@polymer nanospheres would be favorable for STF.

The hard SiO_2 nanospheres were usually used in the STF since their easy preparation and tunable sizes. Many works have been done for developing polymer coated SiO_2 nanospheres, such as SiO_2@poly(methyl methacrylate) (PMMA)[46, 47, 48], SiO_2@polystyrene (PS)[49], SiO_2@poly(3-aminophenylboronic acid)[50], SiO_2@poly(vinyl chloride) (PVC)[51]. Unfortunately, although many works have been done for developing polymer encapsulated SiO_2 nanospheres, there was still no report about the one-step fabrication of the SiO_2@polymer core shell particles and then investigating the STF thereof.

In this work, a one step approach was developed to scale-up synthesize SiO_2@Polydopamine (PDA) inorganic-organic core/shell nanospheres. The shell thickness of the PDA was tunable by varying the concentration of the dopamine precursor. By dispersing the SiO_2@PDA core/shell nanospheres into the polyethylene glycol, the relative STFs were obtained and they exhibited higher ST effects than the SiO_2 based STF. A possible improving mechanism was proposed and it was found that

the PDA shell played a critical role in decreasing the critical shear rate. The as-prepared high performance STF would be widely applied in damper and impact absorbers.

2. EXPERIMENTAL SECTION

2.1. Materials. Tetraethylorthosilicate (TEOS), ethanol and ammonium hydroxide ($NH_3 \cdot H_2O$, 25-28%) were purchased from Sinopharm Chemical Reagent Co. 3-Hydroxytyramine hydrochloride (98%) was purchased from Aladdin. All chemicals were used directly as received without further treatment. Re-distilled water was used in this work.

2.2. The preparation of SiO_2@PDA nanospheres. Scheme 1 illustrates the preparation process of the nanospheres. The synthesis was conducted in a 2000 mL three necked flask, which was fitted with a mechanical stirring. Ethanol (1142mL), distilled water (49.3mL) and ammonium hydroxide (93.2mL) were firstly added to the flask and stirred for 10 min. Then TEOS (53.6mL) was added into the solution dropwise. After 4h, TEOS (26.8mL) and distilled water (24.7mL) was added into the solution. 8 hours later, TEOS (26.8mL) and distilled water (24.7mL) was added into the solution again. The temperature was kept at 40.3℃ by using a Thermostatic Water Bath. 8 hours later, a certain amount of dopamine was introduced into the reaction solution and the reaction was conducted at 25℃ for 24 hours. SiO_2@PDA core/shell nanospheres with different thickness of PDA layer were prepared by varying the dopamine concentration of 1.0g/L (SiO_2@PDA-1), 2.0g/L (SiO_2@PDA-2), 3.0g/L (SiO_2@PDA-3) and 4.0g/L (SiO_2@PDA-4), respectively. The resultants SiO_2/PDA

nanospheres were collected by centrifugation after polymerization. After being rinsed by ethanol and distilled water for three times respectively, the product was dried in a vacuum oven at 50℃.

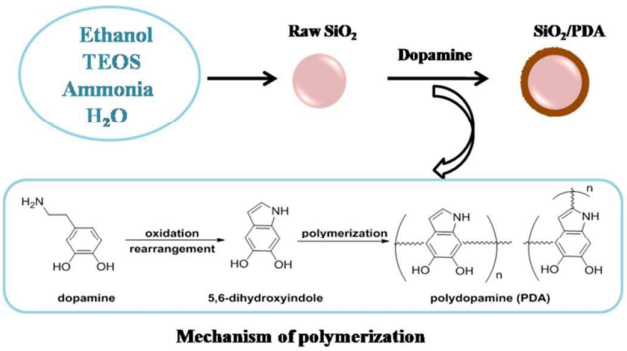

Scheme1. The mechanism and illustration of the synthesis of SiO_2@PDA core/shell nanospheres.

2.3. The preparation of the SiO_2@PDA based STF. Firstly, the SiO_2@PDA was added into poly (ethylene glycol) 200. Then, the mixtures were mixed in a ball crusher in order to obtain homogeneous dispersions. 24 h later, the final product was collected when no terrible aggregation was found in the suspension. Here, the obtained STFs were sealed in a vial before use.

2.4. Rheological measurements. The rheological properties of the STF were measured by using the rheometer (Physical, MCR301, Anton Paar) at 25℃ with cone-plate having a cone angle of 0.2^{o} and a diameter of 25 mm. The rheological properties of each sample were measured under both static and dynamic loading conditions. The steady-shear and oscillatory-shear tests were conducted with a gap size of 0.05mm. In order to remove loading effects, a pre-shear of $1s^{-1}$ was applied for 60 s before collecting the experimental data.

2.5. Characterization. The particle size and macroscopic features were determined by a field emission scanning electron microscope (20 kV, JEOL JSM-6700F SEM). The thickness of the shell was observed by a transmission electron microscopy (TEM, JEM-2011) with an accelerating voltage of 200 kV. Infrared (IR) spectra were measured by a Nicolet Model 759 Fourier transform infrared (FT-IR) spectrometer in the wavenumber range 4000-500cm^{-1} with using a KBr wafer. (XPS, TG) X-ray photoelectron spectra (XPS) were measured on an ESCALAB 250. Thermogravimetric (TG) analysis was performed in air from room temperature to 700℃ at the rate of 10℃/min on a DTG-60H thermogravimetric instrument.

3. RESULTS AND DISCUSSION

3.1. Preparation and characterization of the SiO_2@PDA nanospheres

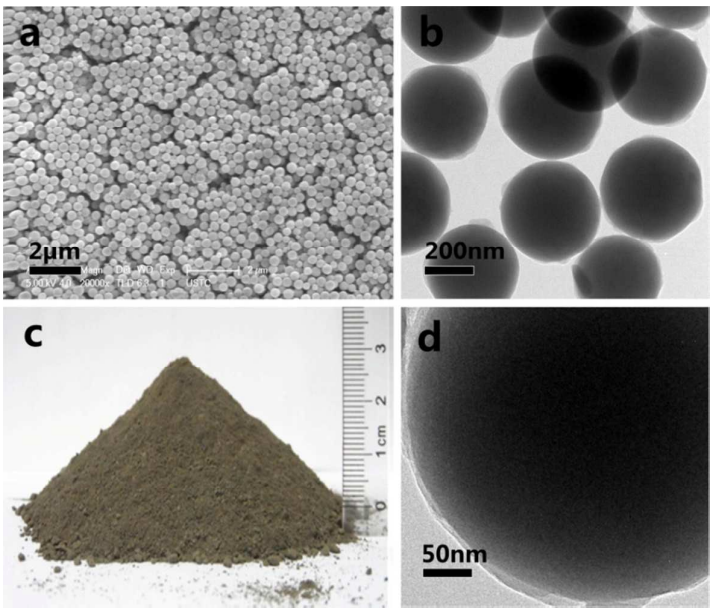

Figure 1. SEM (a) and TEM (b, d) image of the SiO_2@PDA nanospheres synthesized with dopamine concentrations of 2g/L; c is the photograph of one-pot product.

In this one-step synthesis, the SiO_2@PDA nanospheres were obtained by using a modified Stöber reaction. Firstly, SiO_2 nanospheres were formed during the hydrolysis of the TEOS precursor in the alkali medium. As soon as the TEOS was almost completely consumed, the dopamine was added into the solution to coat PDA layer onto the surface of the SiO_2 nanospheres. After rinsing and vacuum heating, the SiO_2@PDA particles were obtained. Because of the simple and green process, this economical method is of high potential in practical application.

Figure 1a shows the SEM image of the SiO_2@PDA product prepared with the DA concentration of 2g/L. All the particles presented the spherical morphology and they were well dispersed without any large aggregation. These nanospheres were uniform and the average size was about 360 nm. The TEM was applied to investigate the inner nanostructure of the SiO_2@PDA nanospheres. Interestingly, beside the black core, there was a thin layer was covered on the surface of the nanosphere, which indicated the SiO_2@PDA nanospheres presented a typical core/shell nanostructure (Figure 1b). The higher magnification TEM image showed that the shell thickness was about 10 nm (Figure 1d). In considering that the DA monomer was added later, the thin shell was indexed to be the PDA. Figure 1c presents the photo of SiO_2@PDA nanospheres prepared in one experiment. The yield of the nanospheres was 32 g in one-pot reaction, which is much larger than most of the previous method for preparing core/shell nanospheres. Moreover, due to the PDA shell, the powder presented gray color, which was different from the white pristine SiO_2.

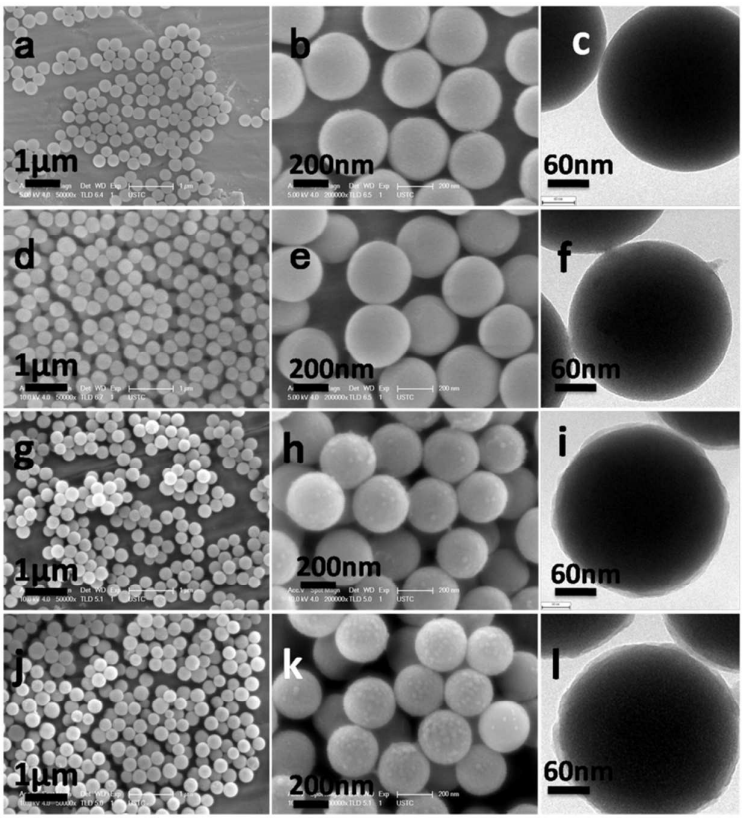

Figure 2. SEM (a, b, d, e, g, h, j, k) and TEM (c, f, i, l) image of the SiO_2 (a, b, c) and SiO_2@PDA nanospheres synthesized with dopamine concentrations of 1g/L (d, e, f), 3g/L (g, h, i), 4g/L (j, k, l).

Since the hydrophilic surface, the PDA can attach to the SiO_2 nanosphere to form core shell nanostructure. With increasing of the DA concentration, the PDA shell thickness increased. Figure 2a-l showed the SEM and TEM images of the pristine SiO_2 (a-c) and SiO_2@PDA (d-l) nanospheres. Without the PDA coating, all the SiO_2 particles were spherical and the average size was about 350 nm. A thin layer would appear on the surface of the SiO_2 when the PDA was *in situ* polymerized. The PDA is a low molecule weight polymer and its contrast is lower than the SiO_2, thus it is difficult to distinguish the shell when the shell thickness is thin. Although it is hard to

find the thin PDA shell in the TEM image, the shell is indeed coated on the SiO_2 surface since the powder present gray color. Energy dispersive spectrometer (EDS) mapping spectra of each element on the surface of the SiO_2@PDA core-shell nanoparticles indicate that the layer of polydopamine was encapsulated on the surface of SiO_2 (Figure S2). Additionally, with increasing of the shell thickness, the PDA layer would be clearly presented in the TEM image. In this work, the starting concentration for the dopamine was controlled from 1g/L (d-f) to 3g/L (g-i), 4g/L (j-l). The TEM images indicated the average shell thickness increased from 2nm to 13nm. Different to the smooth SiO_2, the surface of the SiO_2@PDA particles became rough, which was corresponding to the PDA shell. Importantly, the PDA shell was uniformly coated on the SiO_2 nanospheres without shell coalescence, thus the obtained product was monodisperse (Figure S1).

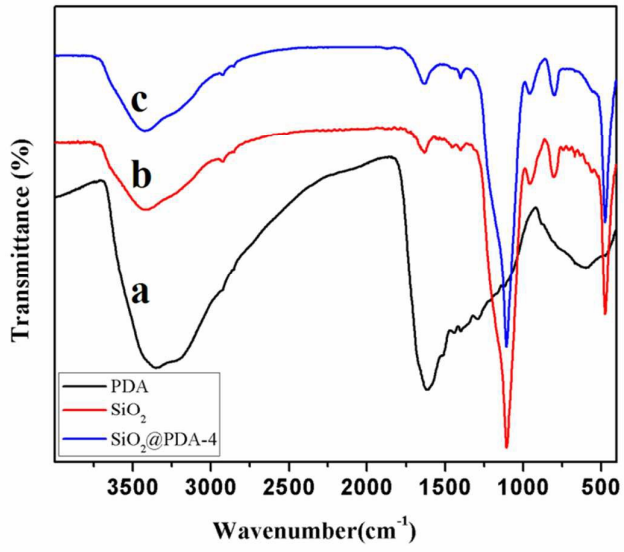

Figure 3. FTIR spectra of (a) dopamine, (b) pristine SiO_2 particles and (c) SiO_2@PDA particles synthesized with 4g/L dopamine concentration.

The FTIR spectra of free dopamine, pristine SiO_2 and SiO_2@PDA nanospheres were investigated. Figure 3a showed the typical FT-IR spectra of polydopamine, which had broad bands in the range between 940 and 1800 cm^{-1} with no distinguishable peaks due to the highly complex structure of polydopamine. The peaks centered at around 3346cm^{-1} was ascribed to the stretching vibration of nitrogen-hydrogen (-NH) /oxygen-hydrogen (-OH) bonds. Because of the low content of the PDA, the SiO_2 (Figure 3b) and SiO_2@PDA (Figure 3c) nanospheres presented similar FTIR spectra. For SiO_2@PDA nanospheres, the strong absorption located at 1104cm^{-1} and 804cm^{-1}, were assigned to the stretching vibrations of silicon-oxygen (-Si-O-) groups.

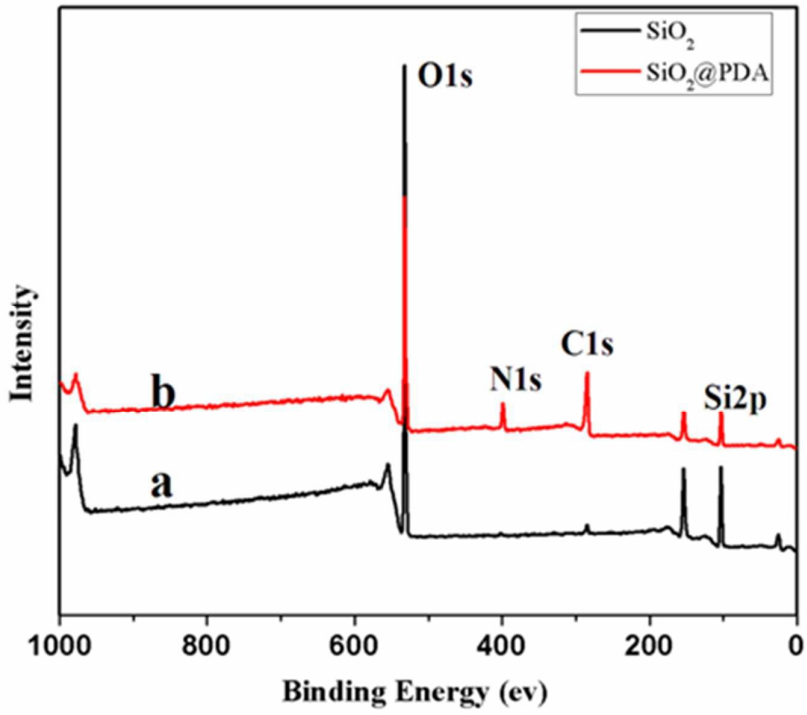

Figure 4. Broad-range XPS spectra of SiO_2 (a) and SiO_2@PDA (b) nanospheres.

The XPS spectra were employed to analyze the surface of the final product. Typically, the strong O1s and Si2p peaks were clearly found in the spectra of SiO_2

nanospheres (Figure 4a). A tiny C1s peaks was presented in the spectra, which may be due to residue ethanol solvent or -OCH_2CH_3 groups in the surface of the SiO_2 nanospheres. Distinctively, for the SiO_2@PDA core shell nanospheres, the nitrogen signal can be clearly observed in Figure 4b. The mole ratio of nitrogen (N1s, 401.8 eV) on the surface of SiO_2@PDA nanospheres was 7.88%. Moreover, the intensity of the C1s peaks was also obviously enhanced. The detective depth of the XPS is about 10 nm and the shell thickness of the PDA is thinner, thus the Si2p signal was also presented in the SiO_2@PDA nanospheres. These results demonstrated the successful coating of the PDA shell on the SiO_2 nanospheres because the N1s and C1s signal in the XPS spectra mainly come from the PDA which contained large amount of amide and benzyl function groups.

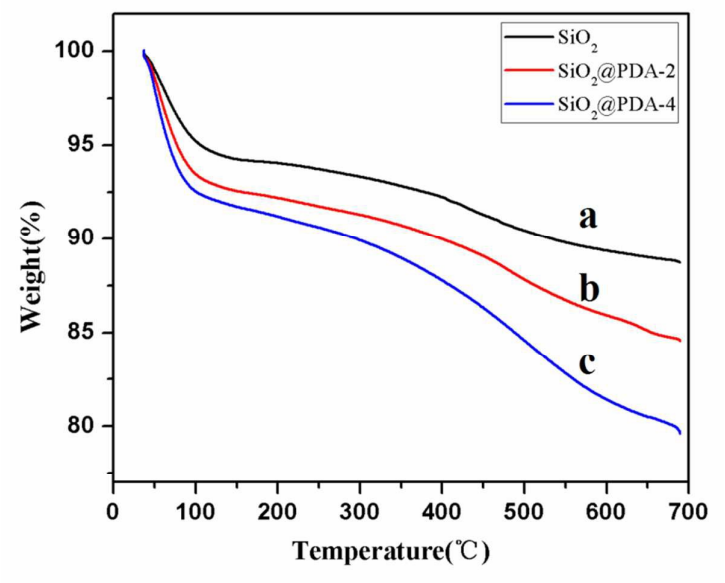

Figure 5. TG of the as prepared SiO_2 particles, SiO_2@PDA-2, and SiO_2@PDA-4 nanospheres, respectively.

As shown in Figure 5a was the thermogravimetric curve of raw SiO_2. The weight loss from 0 to 100℃ was attributed to the adsorbed water. With further increasing the temperature to 500℃, it could be found a slow decrement of the weight loss, which was corresponding to the residue organic groups in the SiO_2 nanospheres. This result also agreed with the XPS analysis. For SiO_2@PDA (b, c), the weight loss in this area clearly increased and it was attributed to the decomposition of the PDA. The gradual weight loss of SiO_2 nanospheres (a), SiO_2@PDA-2 (b), SiO_2@PDA-4 (c) was 11.2%, 15.4% and 19.9%, respectively. The different weight losses between SiO_2@PDA-2 and SiO_2@PDA-4 nanospheres indicated that they had different content of PDA shell. The weight loss increased with increasing of the thickness of the coated layer. In order to give an accurate value of the density of these nanospheres, we performed the solution (double-stilled water) densitometry measurements at different mass fraction by the method of pycnometer. The results indicated that the SiO_2 nanosphere density is =2.05±0.01 g/cm^3, the SiO_2@PDA-2 density is 1.94±0.01 g/cm^3, the SiO_2@PDA-4 density is 1.89±0.01 g/cm^3 (278K). The average density of SiO_2@PDA core shell particles is slightly less than the SiO_2.

3.2. The ST rheology behavior of the SiO_2@PDA nanospheres based STF

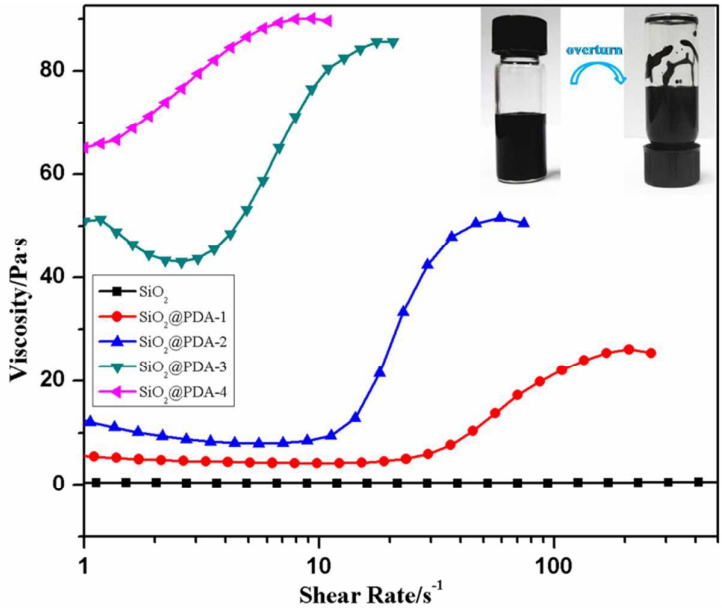

Figure 6. Viscosity vs. shear rate under steady shear mode for SiO_2 and PDA@SiO_2 nanospheres based STFs. The inserted picture illustrated the good fluidity of the PDA@SiO_2 nanospheres based STFs.

After dispersing these SiO_2/PDA core/shell nanospheres into the PEG200 solvent, the dark brown STF was obtained. As shown in Figure 6 (the inserted picture) of the STF. Clearly, the STF is of well fluidity and the core/shell particles are uniformly dispersed within the carrying fluid without large aggregations. Figure 6 presented the static rheological properties of the SiO_2@PDA nanospheres based STFs (58 wt %), in which the SiO_2@PDA nanospheres were of different shell thickness. To better understand the effect of PDA shell, the SiO_2 nanospheres based STF was also prepared. Because of the low mass fraction of 58%, no obvious ST behavior was found in the SiO_2 nanospheres based STF. However, as shown in Figure 6, the SiO_2@PDA-1 based STF presented typical ST behavior and the maximum viscosity

could reach to 26.2 Pa·s. Interestingly, the maximum viscosity of the SiO_2@PDA nanospheres based STFs increased with the thickness of the PDA shell. Moreover, the critical shear rate decreased with increasing the PDA shell thickness and it could decrease to nearly 1 or 2 s^{-1}. Unfortunately, the initial viscosity of the STFs increased from 5.2 to 12.1, 51.2, and 64.8 Pa·s while the relative maximum viscosity was 26.2, 51.6, 86.4, and 90.4 Pa·s, respectively. The SiO_2@PDA-2 based STF has the largest relative increment of the viscosity (about 400%), thus the SiO_2@PDA-2 was considered to be the optimum candidate for the high performance STF.

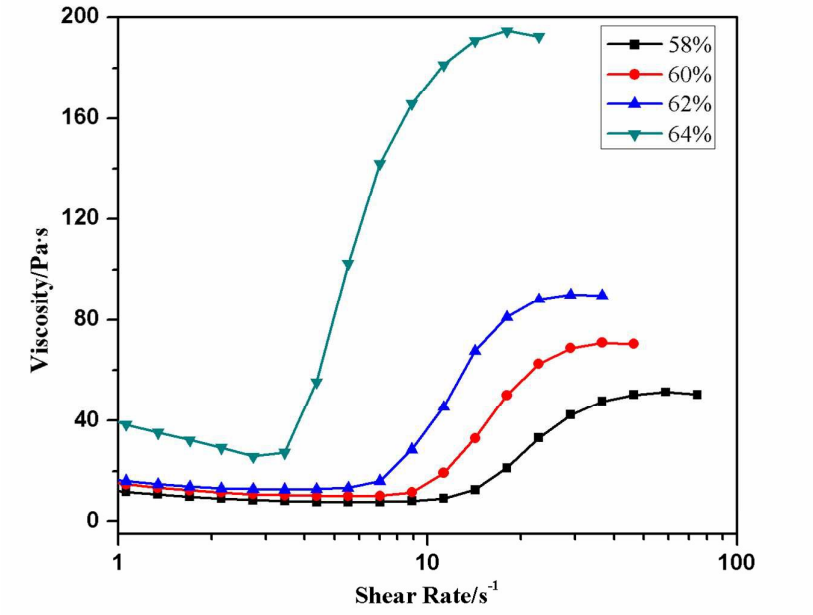

Figure 7. Viscosity vs. shear rate for different mass fractions (64%, 62%, 60% and 58%) suspensions of SiO_2@PDA-2 under steady shear mode.

The influence of shell thickness on the rheological behavior of relative STF was performed by using the SiO_2@PDA-2 as the example. Figure 7 showed the static rheological properties of the SiO_2@PDA-2 based STFs with different mass fractions

(64%, 62%, 60% and 58%). It can be observed that the viscosity curve becomes steeper and the maximum viscosity in ST region increases with the increasing of concentration. When the mass fraction is 58%, the critical shear rate and the maximum viscosity are 12.8 s^{-1} and 51.6 Pa·s, respectively. Once the mass fraction reaches to 64%, the critical shear rate decreases to 2.5 s^{-1} and the maximum viscosity reaches up to 194.6 Pa·s. The critical shear rate is reduced by 5 times approximately, while the maximum viscosity increases about 4 times.

The above results indicated that the critical shear rate was highly dependent on the mass fraction. As the mass fraction increases, the critical shear rate decreases. At the same time, the initial viscosity also increases with the mass fraction increasing. When the mass fraction increased from 58% to 64%, the initial viscosities increased from 12.1 Pa·s to 35.3 Pa·s. The particle concentration is one of the most important factors in controlling the ST behavior of suspensions. Under shear loading, the dispersing particles are pushed into each other. They must overcome the viscous drag forces from the small lubrication gaps between neighboring particles so as to form the hydrocluster. At high concentration, the average distance between two adjacent particles would be shortened and the hydrodynamic force would be easier to move more particles to form larger particle clusters. As a result, the critical shear rate decreases and ST effect enhances as the particle concentration increased.

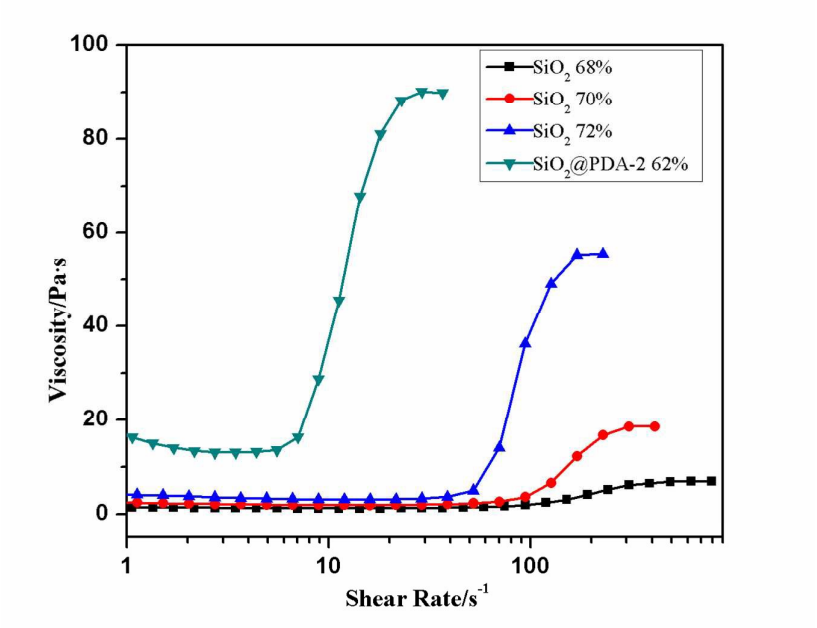

Figure 8. Viscosity vs. shear rate for the SiO_2 nanospheres based STF with different mass fraction (68%, 70% and 72%) and the (62%) SiO_2@PDA-2 based STF

In order to further compare the different rheological properties between the SiO_2 and SiO_2@PDA nanospheres based STF, the influence of mass fraction on the SiO_2 nanospheres based STF was also investigated. Figure 8 showed that the maximum viscosities are 7.3 Pa·s, 18.6 Pa·s, 55.3 Pa·s when the mass fraction were 68%, 70% and 72%, respectively. Similar to the SiO_2@PDA based STFs, the critical shear rate of the SiO_2 based STFs decreased from 155.5 s^{-1} to 95.3 s^{-1}, and 52.9 s^{-1}. Comparable, the maximum viscosity and critical shear rate of the SiO_2@PDA-2 based STF with the mass fraction of 62% are 90.1 Pa·s and 5.7 s^{-1}. It is worth mentioning that the initial viscosity of the SiO_2@PDA-2 based STF (16.1 Pa·s) is higher than the raw SiO_2 nanospheres based STF (approximately 3 Pa·s). Generally, SiO_2@PDA-2 based STF exhibits a better rheological behavior than SiO_2 nanospheres based STF though its concentration is smaller, which demonstrates that the fitted coated layer on the surface of SiO_2 nanospheres improves the rheological behavior of their STFs.

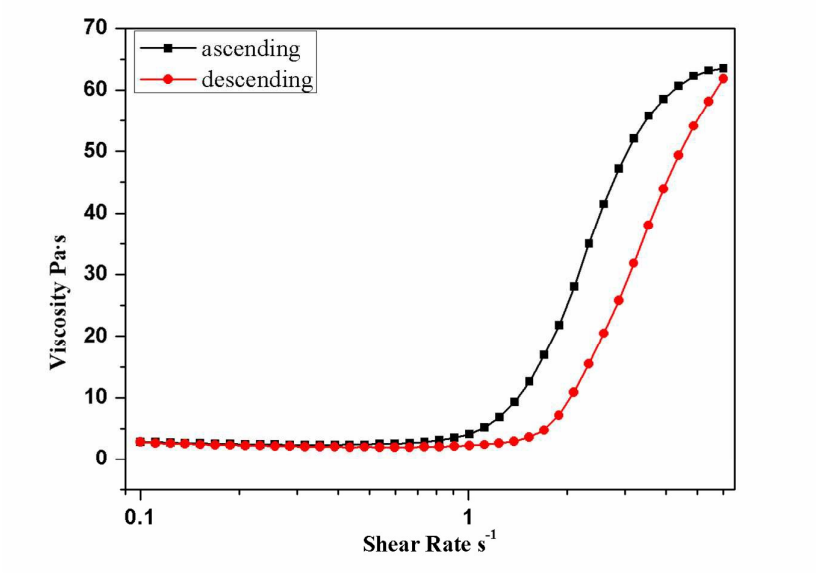

Figure 9. Reversible shear thickening behavior of the SiO_2@PDA-2 based STF with the mass fraction of 61%.

In this work, the reproducibility of shear thickening performance under cyclic loading was investigated. Figure 9 showed the viscosity measured for both ascending and descending shear rate sweeps of SiO_2@PDA-2 based STF with the mass fraction of 61%. There is a slight decrease of viscosity at low shear rate, while it increases quickly as soon as the shear rate reaches the critical shear rate. At the same time, the viscosity decreases immediately when the shear rate decreases. It is necessary to note that the viscosity are in good agreement at the same shear rate, which indicates that the shear thickening behavior of SiO_2@PDA-2 based STF is reversible. The hydroclusters formed in the shear thickening period will decompose and disperse in the dispersed phase again as soon as hydrodynamic lubrication decreased[4]. To this end, we can conclude that the as-prepared shear thickening fluid exhibits excellent cyclic reversibility in ST effect, which is very beneficial for industrial applications.

3.3. Enhancing mechanism for the SiO_2@PDA nanospheres based STF. Based on the above analysis, it can be found that the SiO_2@PDA is superior to the naked SiO_2 in STF, thus the effect of the PDA shell is important for understanding the improving mechanism. As we know, the PDA consists of large amount of hydrophilic hydroxyl and amino groups (Scheme1). Due to these hydrophilic groups, they were compatible to the surface of SiO_2. Because the density of the PDA is lower than the SiO_2, the stability of the SiO_2@PDA particles in the suspension must be much better. Moreover, due to the large amount of the hydroxyl and amino groups on the surface, the SiO_2@PDA core shell particles show higher affinity to the PEG solvent than the naked SiO_2 particles. Moreover, it is well known that the hardness of the PDA is smaller than the SiO_2. After coating the PDA shell, the obtained SiO_2@PDA core shell particle possessed a hard core and a soft shell. The soft PDA shell enhance the lubrication hydrodynamic interaction between the core shell particles, thus in favor of forming particle clusters when the suspension was subjected to shear[27].

According to the hydrocluster mechanism (Scheme 2), random collisions among particles make them naturally resistant to flow to keep an equilibrium state. Under applying an external shear stress (or the shear rate), particles become to be organized in the shear flow, which lowers the viscosity and thus the shear thinning exhibits. If the shear rate reach to a critical value, the hydrodynamic interactions between particles occupies the main position and led the random dispersion of particles to form spawn hydroclusters (red). In this case, the suspension presents a transient fluctuation, thus the viscosity abruptly increase. This phenomenon is named as shear thickening.

The surface properties of the dispersed particles play an important role in the rheology of the dense suspension[52, 2, 53]. It is well known that there are large amounts of hydrophilic hydroxyls and amino groups of PDA. The PDA layer can be used as an intermediate to anchor functional molecules on the surface through chemical bonds or other physical bonds (hydrogen bond or van der Waals' force), which indicates that the surface of PDA layer is abundant of hydroxyls and amino groups[54, 55, 56]. Hydroxyl groups and amino groups can form hydrogen bonds with certain polar molecules[57, 58]. It is rational to speculate hydrogen bonds have been formed between nanospheres and polyethylene glycol 200. Furthermore, the interaction of hydrogen bonds is common in the explanation of the mechanism of shear thickening[53, 59]. In SiO_2@PDA core shell particles based STF, due to large amount of hydroxyls on the particles surfaces, the particle interactions are enhanced by the hydrogen bonds between particles. Therefore, hydroclusters formed in the SiO_2@PDA core shell particles based STF must be larger than the SiO_2 based STF.

The weight percentage of the dispersing particles in the STFs was kept as a constant in this work. Due to the low average density of the SiO_2@PDA core shell particles, the particles volume ratio of was larger than the SiO_2. Under the same shear rate, the SiO_2@PDA core shell particles must be easier to form hydroclusters than the SiO_2 particles due to the smaller inter-particles distance. Therefore, the critical shear rate for the SiO_2@PDA particles based STFs was smaller than the SiO_2 particles. With increasing of the shell thickness, the density further decreased. To this end, the critical shear rate increased with decreasing the shell thickness. Moreover, more particles

would be presented in the thicker PDA shell thickness based STFs, thus the relative initial viscosity would increase. However, the weight percentage of the PDA in the core shell particles is very small (about 5 wt% for SiO_2@PDA-2). The number of the particles in 62% SiO_2@PDA-2 STF was smaller than the one in the 72% SiO_2 STF, while it presented better ST effect. Thus, both increment of the particle volume ratio and the surface inter-force synergistically contributed to the enhancing ST effects. Here, the surface property played the key role in determining the initial viscosity and critical shear rate in the STF.

The hardness of the dispersing particles is also very important in the STFs because the harder particles can resist larger forces without being broken [25, 27]. It was reported that the higher cross-linking density of the PSt-EA particles presented better the ST effect. For this SiO_2@PDA based STF, the hard SiO_2 enable the core shell particles to form stable hydroclusters under applying the external shear force, thus exhibited large maximum viscosity. From the SEM and TEM of pristine SiO_2 and SiO_2@PDA nanospheres (Figure 2 and Figure S1), we can observe that the surface of SiO_2@PDA nanospheres become rougher than that of pristine SiO_2 clearly. The result is consistent with previous report[41]. Although the total amount of the PDA layer is relatively small, the polymer layer is fluffy and the surface area of nanospheres becomes larger with the roughness increase. As to discussions about the role of friction forces in shear thickening field, many works have been done[60-66]. Due to the increase of surface area and roughness of SiO_2@PDA nanospheres compared with pristine SiO_2, the friction coefficient μ between the particles increases. Therefore we speculate that

particle-particle inter-forces increases simultaneously under certain shear rate, which contributes to stabilize the hydroclusters. Based on above analysis, we can conclude that the particle with a hard core and soft shell is an ideal candidate for high performance STF. An optimum shell thickness can lead to the best ST effect in one system. The surface property of the core shell particles highly affected the inter-forces between the particles thus further influenced the relative ST effect.

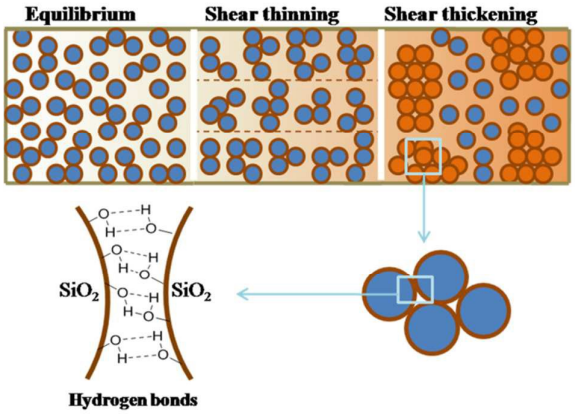

Scheme 2. The diagrammatic illustrates the change in microstructure of the transitions from equilibrium to shear thinning and shear thickening in the core-shell particles' suspension and the hydrogen-bond interaction among the surfaces of the particles.

4. CONCLUSIONS

In this work, a simple in situ polymerization method was introduced to scale-up synthesize core shell SiO_2@PDA nanospheres which can be used for preparing high performance STFs. The rheological properties of the STFs thereof were highly dependent on the PDA shell thickness. With increasing of the shell thickness, the initial shear rate decreased and the maximum viscosity increased. Under the optimum parameter, the maximum viscosity of the STF reached up to 194.6 Pa·s. The

SiO_2@PDA core-shell nanospheres based STF presented better ST effect than the naked SiO_2 and a possible enhancing mechanism was analyzed. It was found that increment of the surface inter-force play the dominant role in determine the ST effect, while particle number and hardness also synergistically contributed to the enhancing ST effects. This hard core/soft shell type composite particle based STF will be useful in not only the fundamental study but also in engineering applications.

ACKNOWLEDGMENTS

Financial supports from the National Natural Science Foundation of China (Grant Nos. 11372301), The Fundamental Research Funds for the Central Universities and the National Basic Research Program of China (973 Program, Grant No. 2012CB937500) are gratefully acknowledged. This study was also supported by the Collaborative Innovation Center of Suzhou Nano Science and Technology.

REFERENCES

1. E. Brown and H. M. Jaeger, *Rep Prog Phys*, 2014, **77**, 46602.
2. E. Brown, N. A. Forman, C. S. Orellana, H. Zhang, B. W. Maynor, D. E. Betts, J. M. DeSimone and H. M. Jaeger, *Nat Mater*, 2010, **9**, 220-224.
3. R. Seto, R. Mari, J. F. Morris and M. M. Denn, *Phys Rev Lett*, 2013, **111**, 218301.
4. H. A. Barnes, *J Rheol (1978-present)*, 1989, **33**, 329-366.
5. X. Z. Zhang, W. H. Li and X. L. Gong, *Smart Mate Struct*, 2008, **17**, 35027.
6. T. J. Kang, C. Y. Kim and K. H. Hong, *J Appl Polym Sci*, 2012, **124**, 1534-1541.
7. M. Soutrenon and V. Michaud, *Smart Mater Struct*, 2014, **23**, 35022.
8. C. Heussinger, *Phys Rev E*, 2013, **88**, 50201.
9. J. W. Bender and N. J. Wagner, *J Colloid Interf Sci*, 1995, **172**, 171-184.

10. D. P. Kalman and N. J. Wagner, *Rheol Acta*, 2009, **48**, 897-908.

11. X. Cheng, J. H. McCoy, J. N. Israelachvili and I. Cohen, *Science*, 2011, **333**, 1276-1279.

12. B. J. Maranzano and N. J. Wagner, *J Chem Phys*, 2002, **117**, 10291-10302.

13. R. Gamez-Corrales, J. Berret, L. M. Walker and J. Oberdisse, *Langmuir*, 1999, **15**, 6755-6763.

14. W. Jiang, Y. Sun, Y. Xu, C. Peng, X. Gong and Z. Zhang, *Rheol Acta*, 2010, **49**, 1157-1163.

15. S. S. Shenoy and N. J. Wagner, *Rheol Acta*, 2005, **44**, 360-371.

16. X. Q. Liu, R. Y. Bao, X. J. Wu, *RSC Adv*, 2015, **5**, 18367-18374.

17. E. Brown, H. Zhang, N. A. Forman, B. W. Maynor, D. E. Betts, J. M. DeSimone and H. M. Jaeger, *Phys Rev E*, 2011, **84**, 31408.

18. E. Brown, H. Zhang, N. A. Forman, B. W. Maynor, D. E. Betts, J. M. DeSimone and H. M. Jaeger, *J Rheol (1978-present)*, 2010, **54**, 1023-1046.

19. K. Yu, H. Cao, K. Qian, X. Sha and Y. Chen, *J Nanopart Res.*, 2012, **14**, 1-9.

20. G. V. Franks, Z. Zhou, N. J. Duin and D. V. Boger, *J Rheol (1978-present)*, 2000, **44**, 759-779.

21. A. Zupančič, R. Lapasin and G. Torriano, *Prog Org Coat*, 1997, **30**, 79-88.

22. E. B. Bagley and D. D. Christianson, *J Texture Stud*, 1982, **13**, 115-126.

23. L. Chang, K. Friedrich, A. K. Schlarb, R. Tanner, L. Ye, *J Mater Sci*, 2011, **46**, 339-346.

24. Y. Otsubo, M. Fujiwara, M. Kouno and K. Edamura, *Rheol Acta*, 2007, **46**, 905-912.

25. D. P. Kalman, R. L. Merrill, N. J. Wagner and E. D. Wetzel, *ACS Appl Mater Inter*, 2009, **1**, 2602-2612.

26. A. Le Grand and G. Petekidis, *Rheol Acta*, 2008, **47**, 579-590.

27. W. Jiang, F. Ye, Q. He, X. Gong, J. Feng, L. Lu, S. Xuan, *J Colloid Interf Sci*, 2014, **413**, 8-16.

28. S. Ullah, E. P. Ferreira-Neto, A. A. Pasa, C. C. Alcântara, J. J. Acuña, S. A. Bilmes, M. L. M. Ricci, R. Landers, T. Z. Fermino and U. P. Rodrigues-Filho,

Appl Catal B-Environ, 2015, **179**, 333–343.

29. X. Liu, N. Wu, C. Cui, *RSC Adv*, 2015, **5**, 24016-24022.
30. J. B. Li, S. J. Zhang, J. Liang, *RSC Adv*, 2015, **5**, 7994-8001.
31. J. Feng, W. Qin, Y. Ju, *RSC Adv*, 2015, **5**, 53514-53523.
32. J. T. McKeown, Y. Wu, J. D. Fowlkes, P. D. Rack and G. H. Campbell, *Adv Mater*, 2015, **27**, 1060-1065.
33. N. Iqbal, A. Afzal, A. Mujahid, *RSC Adv*, 2014, **4**, 43121-43130.
34. Z. Li, A. Wang, C. Guo, Y. Tai and L. Qiu, *Dalton T*, 2013, **42**, 13948-13954.
35. Y. J. Hong, M. Y. Son and Y. C. Kang, *Adv Mater*, 2013, **25**, 2279-2283.
36. D. Kim, Y. Tian, H. J.Choi, *RSC Adv*, 2015, **5**, 81546-81553.
37. R. Ghosh Chaudhuri and S. Paria, *Chem Rev*, 2011, **112**, 2373-2433.
38. C. Jo, H. J. Lee and M. Oh, *Adv Mater*, 2011, **23**, 1716-1719.
39. R. Tayebee, M. M. Amini, H. Rostamian and A. Aliakbari, *Dalton T*, 2014, **43**, 1550-1563.
40. M. L. Breen, A. D. Dinsmore, R. H. Pink, S. B. Qadri, B. R. Ratna, *Langmuir* 2001, **17**, 903-907.
41. Z. Xia, Z. Lin, Y. Xiao, L. Wang, J. Zheng, H. Yang and G. Chen, *Biosens Bioelectron*, 2013, **47**, 120-126.
42. C. Jo, H. J. Lee and M. Oh, *Adv Mater*, 2011, **23**, 1716-1719.
43. Y. Ma, M. Qiao, C. Hou, Y. Chen, M. Ma, H. Zhang and Q. Zhang, *RSC Adv*, 2015, **5**, 103064-103072.
44. R. Liu, Y. Guo, G. Odusote, F. Qu and R. D. Priestley, *ACS Appl Mater Inter*, 2013, **5**, 9167-9171.
45. Y. Hu, T. Zhao, P. Zhu, X. Liang, R. Sun and C. Wong, *RSC Adv*, 2015, **5**, 58-67.
46. R. Palkovits, H. Althues, A. Rumplecker, B. Tesche, A. Dreier, U. Holle, G. Fink, C. H. Cheng, D. F. Shantz and S. Kaskel, *Langmuir*, 2005, **21**, 6048-6053.
47. K. Ohno, T. Morinaga, K. Koh, Y. Tsujii and T. Fukuda, *Macromolecules*, 2005, **38**, 2137-2142.
48. H. Sertchook and D. Avnir, *Chem Mater*, 2003, **15**, 1690-1694.
49. Y. P. Zhang, S. H. Lee, K. R. Reddy, A. I. Gopalan and K. P. Lee, *J Appl Polym*

Sci, 2007, **104**, 2743-2750.

50. X. Xie, R. K. Li, Q. Liu and Y. Mai, *Polymer*, 2004, **45**, 2793-2802.
51. P. Xu, H. Wang, R. Lv, Q. Du, W. Zhong and Y. Yang, *J Polym Sci Poly Chem*, 2006, **44**, 3911-3920.
52. S. X. Ma and S. L. Cooper, *J Rheol* (1978-present), 2002, **46**, 339-350.
53. B. Chu, A. T. Brady, B. D. Mannhalter and D. R. Salem, *J Phys D: Appl Phys*, 2014, **47**, 335302.
54. H. Lee, S. M. Dellatore, W. M. Miller and P. B. Messersmith, *Science*, 2007, **318**, 426-430.
55. L. Zongguang, Q. Shuxin and W. Jie, *Prog Chem*, 2015, **27**, 212-219.
56. C. Ho and S. Ding, *J Biomed Nanotechnol*, 2014, **10**, 3063-3084.
57. S. R. Raghavan, H. J. Walls and S. A. Khan, *Langmuir*, 2000, **16,** 7920-7930.
58. F. J. Galindo-Rosales and F. J. Rubio-Hernandez, *Appl Rheol*, 2010, **20**, 22781-22787.
59. J. Warren, S. Offenberger, H. Toghiani, C. U. Pittman Jr, T. E. Lacy and S. Kundu, *ACS Appl Mater Inter*, 2015, **7**, 18650-18661.
60. R. Mari, R. Seto, J. F. Morris and M. M. Denn, *J Rheol (1978-present)*, 2014, **58**, 1693-1724.
61. L. E. Silbert, D. Ertaş, G. S. Grest, T. C. Halsey and D. Levine, *Phys Rev E*, 2002, **65**, 31304.
62. M. Jerkins, M. Schröter, H. L. Swinney, T. J. Senden, M. Saadatfar and T. Aste, *Phys Rev Lett*, 2008, **101**, 18301.
63. L. E. Silbert, *Soft Matter*, 2010, **6**, 2918-2924.
64. C. Heussinger, *Phys Rev E*, 2013, **88**, 50201.
65. R. Seto, R. Mari, J. F. Morris and M. M. Denn, *Phys Rev Lett*, 2013, **111**, 218301.
66. N. Fernandez, R. Mani, D. Rinaldi, D. Kadau, M. Mosquet, H. Lombois-Burger, J. Cayer-Barrioz, H. J. Herrmann, N. D. Spencer and L. Isa, *Phys Rev Lett*, 2013, **111**, 108301.

Abstract Graphic

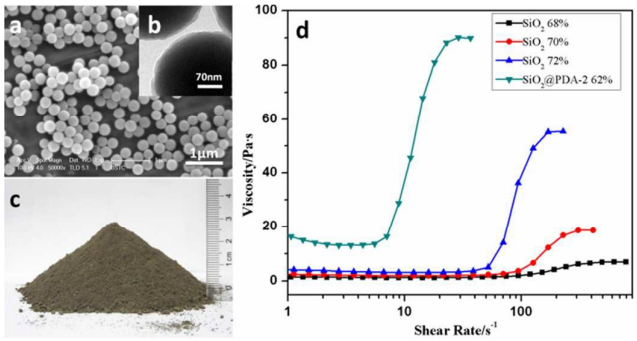

Figure The illustration of the synthesis of SiO_2@PDA core/shell nanospheres and the fitted coated layer on the surface of SiO_2 nanospheres improves the rheological behavior of their STFs.